A Compact 38 GHz Millimetre-Wave MIMO Antenna Array for 5G Mobile Systems

Ashraf Tahat, Bandar Ersan, Laith Muhesen, Zaid Shakhshir
Department of Communications Engineering
Princess Sumaya University for Technology, Amman, Jordan

Talal A.Edwan
Department of Computer Engineering
Princess Sumaya University for Technology, Amman, Jordan

Abstract: This paper presents the design of a compact 2x2 microstrip antenna array of size 11.9x15.3 mm² operating at the mm-wave region of 38 GHz. We achieved a high gain of 14.58 dB, a return loss of -17.7 dB, and a wide impedance bandwidth of 500 MHz. This antenna is duplicated twelve times around an angle of 30° forming a low-profile dodecagon. Each sector can cover a beam of 58° to obtain 12 beams covering the 360 degrees. When compared with implemented antenna designs in the literature that target similar features of compact size and low profile at the desired 5G frequency of 38 GHz, our design had a noticeable reduction in size with an increased gain. Our designed antenna is suited for MIMO beamforming, or switched beam technology applications in mobile wireless systems that include miniaturized base stations or moving network systems, such as mobile hotspots or vehicular networks and related elements.

Keywords: 5G, mmWave, MIMO, compact antenna, antenna array

Introduction

Recent technology trends demonstrate that wireless and mobile communications technologies are blooming at a very rapid rate. It is believed that 5G wireless systems will have greatly enhanced performance reflected in data rates and channel capacity (Mattisson, 2018). Enablers of these high performance systems are contemporary design techniques and principles such as: millimetre-wave (mmWave) technology, massive multiple-input-multiple-output, and sophisticated modulation and coding schemes (Sahoo *et al.*, 2019). Due to limited availability of frequency spectrum resources and propagation challenges

http://doi.org/10.18080/jtde.v8n3.299

(Rappaport *et al.*, 2017) at the newly offered frequency bands, efficient utilization of these bands will require deployment of new configurations of multi-antenna systems incorporating beamforming or an antenna array with switched multibeams in these 5G systems. In addition, various everyday systems with drastically different technical requirements are being redesigned to incorporate 5G wireless systems as the primary means for functionality. As such, these include the general Internet of Things (IoT), where billions of devices will be connected and operated relying on wireless 5G systems. Among these various systems, of special importance, are moving network (MN) systems for 5G vehicular communications, that will include applications such as mobile hotspots (Kim *et al.*, 2019; Sahoo *et al.*, 2019). In addition, it is anticipated that within these MN 5G systems, transportation traffic communications will be delivered in point-to-multipoint topologies (Hong *et al.*, 2017; Muirhead, Imran & Arshad, 2016; Wu *et al.*, 2018).

In order to achieve these special-purpose communications topologies, several techniques have been employed. The most prevalent one is spatial or frequency diversity in conjunction with a compact MIMO antenna array. Alternately, this topology is accomplished utilizing multi-beam antenna arrays employed in forming a desired number of concurrent or dynamic switchable but autonomous high-gain directive beams (Hong *et al.*, 2017; Muirhead, Imran & Arshad, 2016; Wu *et al.*, 2018). However, these applications with special communications topologies require compact low-profile multi-beam antenna arrays with multi-feeding ports for use in this context. Thus, the demand for diverse types of advanced antennas with high-performance designs is increasing exponentially in a similar fashion to the accompanying circuits. However, it is often difficult to meet stringent design requirements on bandwidth, radiation pattern, compact size, and cost of the 5G mobile communications networks with most conventional techniques (Yaacoub, Husseini & Ghaziri, 2016). An antenna of the microstrip patch antenna type (Fadamiro *et al.*, 2019; Al Issa, Khraisat & Alghazo, 2020) can have several merits including a low-profile structure, moderate or high gain, high efficiency, low cost, easy fabrication, in addition to robustness. In recent years, for 5G mobile communications, a few researchers have proposed a number of assorted antenna designs. However, the design intricacy such as large size (Al-Tarifi, Sharawi & Shamim, 2018) and ramification accompanied by low antenna gain and low efficiency are a principal impediment affiliated with them (Verma *et al.*, 2016).

We review some of the compact designs that have been put forward recently in the related literature. The authors in (Verma *et al.*, 2016) have presented a small microstrip patch antenna that was designed for 5G communication systems operating at 10.15 GHz that has a size of 10.2 mm by 7 mm with a narrow long rectangular slot. The used substrate is FR4, which has a dielectric constant of 4.4 and a thickness of 1.6 mm. The antenna is fed using

http://doi.org/10.18080/jtde.v8n3.299

microstrip edge feeding with a lumped port. This antenna achieved a moderate gain of 4.46 dB with an omnidirectional radiation pattern and resonated at 10.15 GHz with a return loss of -18.27 dB with a bandwidth of 400 Hz. In (Ali, Haraz & Alshebeili, 2016), a Dual-Band printed slot antenna was designed for 5G wireless communication systems that resonates at 28/38 GHz using an elliptical patch with an elliptical slot using a proximity feeding technique on the other side of the substrate. The feed line also has a slot in it, which is rectangular in shape. The substrate used has a dielectric constant of 2.2 and a thickness of 0.127 mm. This antenna achieved a return loss of -45 dB at 28 GHz and -22 dB at 38 GHz. At 28 GHz, the gain is 3.63 with a relatively flat pattern, and 4.45 dB at 38 GHz, also with a relatively flat pattern. A compact dual-band antenna array for millimetre massive MIMO applications was designed in (Ali & Sebak, 2016). This antenna array resonates at 28/38 GHz. Each array consists of eight elements designed using 1-to-2 Wilkinson Power Divider. For massive MIMO applications, a total of twelve arrays are mounted around a cylinder achieving a beam scanning of around 40° at 28 GHz and 30° at 38 GHz. Two substrates were used in the design; the first low permittivity substrate (2.2) has the elliptical patches etched onto it, while the second one has a high permittivity substrate (10.2) with the feeding network etched onto it, thus eliminating any radiation interference caused by the feeding network, as there is a ground plane between the feeding network and the arrays separating their radiations. At 28 GHz, the return loss is about -18 dB, and the gain is 12.07 dB; while at 38 GHz the return loss is -28 dB and the gain is 13.46 dB. The size of each antenna array is 13×20 mm, thus giving a diameter for the ellipse of 50 mm. In (Chen & Zhang, 2013), the antenna design approach uses standard PCB technology on a FR4 substrate (dielectric constant = 4.4). The microstrip grid array is printed directly on the substrate. The antenna has a size of 15×15 where the design achieved an impedance bandwidth of 7.16 GHz, and a realized gain of 12.66 dBi at 29.2 GHz. The printed array consists of eight rectangular meshes. Each rectangle is excited from both sides, and thus radiates at two frequencies; the long side operates as a trans-mission line, while the short side is responsible for both the transmission lines and the radiating element.

Here, in this paper, we present a novel design of a compact and low-profile antenna that operates at a selected popular millimetre-wave frequency of 38 GHz that meets the requirements of 5G cellular systems, with special interest for applications of MN systems and miniature base stations or access points. This compact design was achieved through the use of a compact 2 2 microstrip antenna array of size 11.9×15.3 mm² operating at 38 GHz. In spite of the fact that the antenna is small and compact, it has relatively high performance, where we have achieved a high gain of 14.58 dB, a return loss of -17.7 dB, and a wide impedance bandwidth of 500 MHz. This microstrip antenna array was duplicated twelve

http://doi.org/10.18080/jtde.v8n3.299

times around an angle of 30°forming a *dodecagon*. With a total of 48 antenna elements, many challenges arose to overcome the obstacles of millimetre-waves. Utilizing the High Frequency Structured Simulator (HFSS) software, the antenna design simulation and optimization was performed. This design builds on the previously mentioned designs in its compact size when compared with the design in (Ali & Sebak, 2016). However, our design achieved better values in terms of the gain and return loss when compared to the designs discussed above. In the following sections, we describe the details of the design of the MIMO antenna array and its aspects, in addition to obtained results for verification of design parameters and requirements.

Design of the MIMO Antenna Array

In designing an antenna array, the overall results are directly linked to the design of the single element. The patch shape that was chosen held various critical points to keep in mind: return-loss, gain, bandwidth, and design complexity. Working on a design for the desired high frequency range, the decision was to choose a rectangular shape, which held high return loss values, high gain values, and high bandwidth, in addition to having moderate design complexity relative to other shapes. In other words, if a single element antenna has a high gain, narrow bandwidth, and high directivity, an array consisting of duplicates of that element achieves results that are directly dependent on that of the single element. Therefore, a single element was designed and optimized to achieve the best results, then duplicated into a number of arrays. All microstrip antennas consist of at least three layers – where the first layer is a ground plane that simply is a reference to the antenna, above which is the substrate mounted directly between the other two layers, and the top most layer is the microstrip patch. This layer is responsible for radiation to transmit or receive signals. Between the top and bottom layers comes the substrate. The substrate has a thickness that separates the two other layers, and holds the qualities that directly affect the fringing fields.

The substrate

The substrate holds two key parameters: the dielectric constant, and the thickness. In general, as the thickness increases, the resonant frequency increases and the bandwidth decreases. Furthermore, as the thickness of the substrate increases, the fringing field increases, which leads to a decrease in the resonant frequency and an improvement on the return-loss and bandwidth. The dielectric constant defines the amount of energy a material can store in an electric field: increasing the dielectric constant to a point leads to a less efficient and smaller bandwidth radiating antenna. Since the substrate has the ground plane on the opposite side of the antenna, width and length of the substrate are equal to those of the ground. Due to desired design criteria in target applications, a high performance and

http://doi.org/10.18080/jtde.v8n3.299

supportive substrate is to be implemented as the second layer. This will have a pronounced effect on the characteristics of the antenna, especially on the fringing fields, which leads to either improper or beneficial proper radiation. It has to be taken into account that, as both substrate thickness and permittivity change, the radiation behaviour of the fringing fields will be affected (Mishra, Kuchhal & Kumar, 2015), as well as the bandwidth and the efficiency. With a low dielectric constant and low dispersion, Rogers RT/Duroid 5880 (Rogers Corporation, 2018) was selected as the most suitable substrate for its superior performance in preserving the efficiency, and not including any higher modes which would hamper radiation.

The effective dielectric constant

The effective dielectric constant links the dielectric constant to the width and the ratio of width to height of the dielectric constant. The following equation can be used to calculate it:

$$\varepsilon_{eff} = \frac{\varepsilon_r+1}{2} + \frac{\varepsilon_r-1}{2}[1 + 12\frac{h}{w}]^{1/2} \quad (1)$$

Substituting in (1) yields $\varepsilon_{eff} = 2.0918$.

The length

The length of the antenna is a parameter that determines the operating frequency when excited. In general, the length is usually about $\lambda/2$; where $\lambda = c/f$. Using the equation below, the exact length can be found as follows:

$$L_{eff} = \frac{C_0}{2f_r\sqrt{\varepsilon_{\text{eff}}}} - 2\Delta L \quad (2)$$

Note that the length should be slightly less than a half wavelength. But, due to the fringing effect, it looks physically greater in size, and the antenna's length must be increased by an amount of ΔL, as the equation below shows (Samarthay, Pundir & Lal, 2014):

$$\Delta L = 0.412\frac{(\varepsilon_{eff}+0.3)(\frac{w}{h}+0.264)}{(\varepsilon_{eff}-0.258)(\frac{w}{h}+0.8)} \quad (3)$$

Therefore, the length is now equal to the difference between the two equations above, (2) and (3), as follows:

$$L = \frac{C_0}{2f_r\sqrt{\varepsilon_{\text{eff}}}} - 2\Delta L - 0.412\frac{(\varepsilon_{eff}+0.3)(\frac{w}{h}+0.264)}{(\varepsilon_{eff}-0.258)(\frac{w}{h}+0.8)} \quad (4)$$

After the length is found to be equal to 3.1206 mm, the next step is to choose a proper excitation point.

http://doi.org/10.18080/jtde.v8n3.299

The width

The width plays a direct role in bandwidth and return loss: as the width of the microstrip antenna increases, the bandwidth and the return loss increase. However, continuing to increase the width will lead to a point beyond which the bandwidth would be drastically decreased and cause a deviation in the resonance frequency as well (Milligan, 2005). With that in mind, below is the equation used to calculate the width:

$$W = \frac{C_0}{2f_r}\sqrt{\frac{2}{\varepsilon_r+1}} \quad (5)$$

Using (5), the width can be found as W= 2 5956 mm.

The feeding

Our design targets an impedance value of 50 Ω. Since Z=V/I, and the current increases around the centre, the input impedance is greatest at the edges and least at the centre. There are a number of methods to achieve matched input impedance, including aperture couple feeding, coaxial feeding, and inset feeding. In inset feeding, manufacturing will be simpler when compared to other techniques, as well as the size of the overall antenna will not be greatly affected. When the feed is placed directly to the edge of the patch, this gives rise to high input impedance. Therefore, the Inset Feeding method is used in order to minimize the input impedance, where the inset has to be modified by bringing it more towards the centre. The gap on either side of the microstrip line equals its width. This method is useful because it can be directly printed to the antenna board, and where the input impedance can be decreased up to 50%. The position where the inset feed point should be inserted can be found by calculating Z_0.

$$Z_0 = R_{in} * cos^2\left(\frac{\pi}{L_p} - d\right) \quad (6)$$

Moreover, varying the inset length would affect the performance as well, but the inset gap has wider effect on the parameters.

Substrate and ground size

The substrate and ground size affect the efficiency and the bandwidth, as well as the size of the microstrip antenna. The substrate itself has an effect on miniaturization as well as broadbanding the antenna. Furthermore, the ground plane can be used to improve the pattern symmetry, as it can alter the far field pattern shape. In addition, the ground plane also works to avoid and absorb reflections off the ends of the model (Milligan, 2005). With

http://doi.org/10.18080/jtde.v8n3.299

that in mind, the size of the substrate and the ground plane must be greater than that of the patch antenna, and is calculated using the equations below:

$$L_g = 6h + L \tag{7}$$

$$W_g = 6h + W \tag{8}$$

Both the ground plane and the substrate sizes can be found using equations (7) and (8).

Single element results

A design was implemented to verify the integrity of the calculations. Figure 1(a) shows the antenna modelled using the High Frequency Structured Simulator (HFSS) software. For the final antenna design to achieve better results, each variable in the single element design must be optimized. This allows for tuning the deviation in the operating frequency, maximized gain, return loss, and optimized radiation pattern. In order to justify the integrity of the optimized single element results, all characteristics of the antenna will be discussed. a) The resulting gain is 7.95 dB for the optimized single element, which demonstrates its efficient ability to radiate as desired, or, in other words, how well it converts input power into radiating waves heading in a specified direction. Furthermore, the radiation pattern shows no side lobes. Figure 1(b) shows the gain of the single element. b) The achieved return loss was -29.18 dB. This high value of return loss is very desirable and is evidence of the high efficiency of this antenna design, since it is commonly known that this value should be higher than -10 dB in an effective antenna design. Figure 2 shows the single element return loss (in dB) plotted versus frequency.

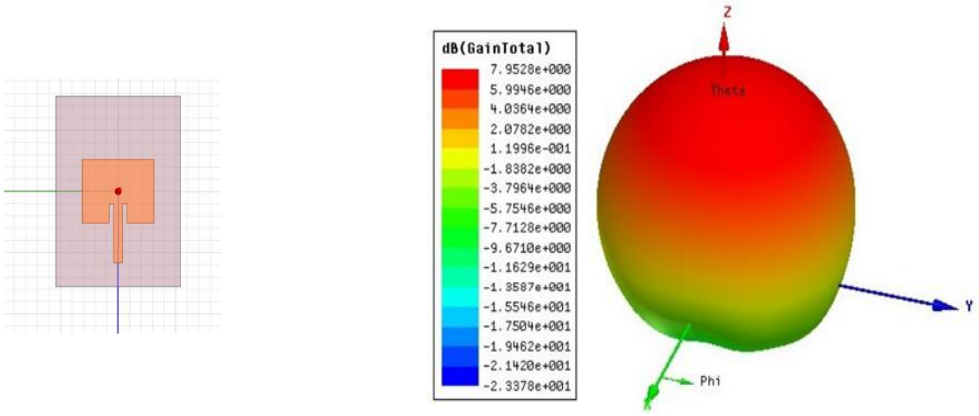

(a) **(b)**

Figure 1. Single Element Antenna (a) Shape (b) 3D Radiation Pattern Showing the Gain.

Array

In this design, the number of antennas was chosen in such a way as to get the optimal desired target parameters without sacrificing the compact size and low profile of the overall

http://doi.org/10.18080/jtde.v8n3.299

antenna. This is because, in an antenna array, the number of antenna elements plays a direct role in the overall performance of the antenna. Using four elements (2×2), the size remained relatively small, while the gain, return loss, and bandwidth greatly improved. Although using sixteen elements (4×4) achieved better gain and return loss, it caused the antenna to be highly directive, therefore having very narrow beam width.

With the single element carrying the optimal characteristics to meet the requirements, it was ready to be duplicated into an array. Each array consisted of four elements with an orientation to favour the beam width, gain, return loss, and size. Pairing too many elements horizontally results in higher gain and return loss, but decreases the beam width drastically, which causes some areas to be unreachable by the antenna. Therefore, the number of antennas mounted horizontally used is two. For vertical elements, as the number of elements increases, the vertical beam width will be decreased drastically. Furthermore, the size of the antenna also increases greatly, as the feedline is directed vertically and requires spacing between elements. Considering the facts above, the number of elements mounted vertically chosen is two elements. Figure 3 shows the design of the (2×2) patch antenna array. Note that the feeding line is positioned to the side of the array, and excited with a lumped port mounted vertically with respect to the substrate of the antenna. This ensures that the design maintains its low profile after the duplication of the elements. Each antenna element has an input impedance of 50Ω. To connect two antenna elements with minimal losses, the two antennas need to be matched using a quarter-wave transformer and a power divider. The power divider, which has a characteristic impedance of 100Ω, is used to ensure that the power delivered to each element is equal.

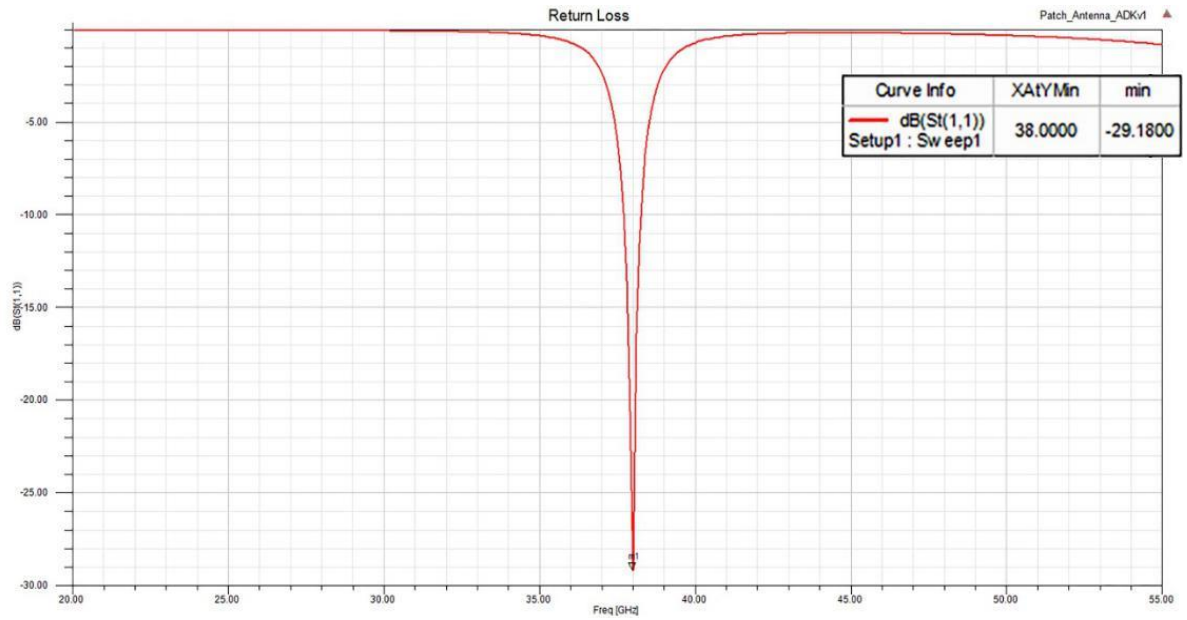

Figure 2. Return Loss of the Single Element Antenna.

http://doi.org/10.18080/jtde.v8n3.299

This power divider can be of any length, including zero length. However, the quarter-wave transformer, used to match the two characteristic impedances, has to exist to match the elements. As seen in the figure above, the quarter-wave transformer's impedance is calculated using $Z_0 = \sqrt{50 \times 100}$. Hence, to achieve a microstrip line with a characteristic impedance of 70.7Ω, the width of the line can be calculated using the two equations (9) and (10) (Milligan, 2005):

$$Z = \frac{Z_0}{2\pi\sqrt{2(1+\varepsilon_r)}} \ln\left(1 + \frac{4h}{w_{eff}}\left(\frac{14+\frac{8}{\varepsilon_r}}{11} + \frac{4h}{w_{eff}} + \sqrt{\frac{14+\frac{8}{\varepsilon_r}}{11} + \pi^2 \frac{1+\frac{1}{\varepsilon_r}}{2}}\right)\right) \quad (9)$$

where

$$w_{eff} = w + t\frac{1+\frac{1}{\varepsilon_r}}{2\pi}\left(1 + \ln\left(\frac{4}{\sqrt{\frac{t^2}{h} + \left(\frac{1}{\pi\frac{w}{t}+1.1}\right)^2}}\right)\right) \quad (10)$$

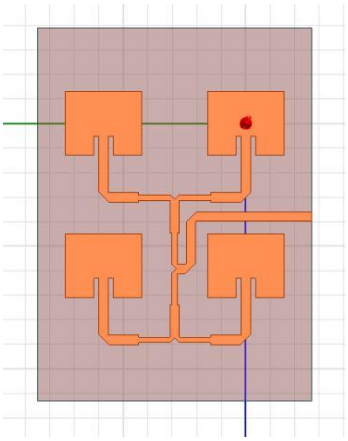

Figure 3. The Proposed 2 × 2 Array.

To reduce power losses, all the 90° corners and all the T-junctions in the feeding network were cut into triangular shape using the method of Mitre Compensation. The following calculations were used to calculate each triangular parameter (Milligan, 2005):

$$x = 0.52 + 0.65 \exp(-1.35\ w/h) \quad (11)$$

All elements on each face were connected to each other using the methodology discussed above. Therefore, to connect the four elements, three quarter-wave transformers were used to match their characteristic impedances.

To ensure that best possible values are achieved using these four element combinations, both the vertical and horizontal spacing between the elements were varied and studied. Table 1 depicts a comparison of the gain, return loss, and operating frequency when varying the spacing. By studying the values in Table 1, the spacing was chosen to favour the gain and the return loss. Therefore, the optimization concluded with a spacing of 6 mm horizontally and 6.5 mm vertically. This also ensures that the overall size of the antenna remains compact.

http://doi.org/10.18080/jtde.v8n3.299

Table 1. Optimization of Element Spacing at Operating Frequency (38 GHz)

Vertical Space	Horizontal Space	Return Loss	Gain
5.5	5.5	-16.94	13.65
6.0	5.5	-22.48	13.76
6.5	5.5	-24.67	13.54
7.0	5.5	-16.77	13.22
7.5	5.5	-15.26	12.90
8.0	5.5	-15.22	12.67
5.5	6.0	-17.51	13.94
6.0	6.0	-25.05	13.65
6.5	**6.0**	**-25.20**	**13.70**
7.0	6.0	-18.29	13.40
7.5	6.0	-17.46	13.13
8.0	6.0	-0.61	12.94
5.5	6.5	-17.31	14.08
6.0	6.5	-26.29	14.04
6.5	6.5	-22.97	13.81
7.0	6.5	-18.04	13.56
7.5	6.5	-18.49	13.36
8.0	6.5	-22.61	13.18
5.5	7.0	-0.61	8.76
6.0	7.0	-21.73	14.09
6.5	7.0	-18.54	13.90
7.0	7.0	-17.49	12.72

Final Antenna Design

The final complete 5G antenna must have multiple excitation points to adhere to the antenna design requirements of MIMO technology. In order to maintain symmetry around the antenna, the antenna must take the shape of either a cylinder or a polygon with multiples of four sides. As the substrate used is not flexible, the proposed design used a polygon. The number of sides used is twelve (dodecagon). This invokes sectoring capabilities into the antenna design, which helps isolate users (in a base station application context) during communication, or multi directional reception beams in a VE. Furthermore, with the use of multiple inputs, the antenna could benefit from beamforming, which helps in delivering and receiving stronger signals when obstacles stand between the two endpoints, as mm-waves have very weak propagation and can be absorbed very easily by obstacles in the environment. To integrate a final design, a total of twelve antenna arrays were used.

Each array is angled at 30° with respect to its adjacent array. This way of mounting the antennas results in a dodecagon (twelve-sided polygon). Simulations of the final antenna design were carried out using HFSS. The final design consisted of 48 antenna elements, divided into 12 arrays such that each array consists of four elements in a 2×2 array configuration. The substrate, Rogers RT/Duroid 5880, is very thin, with a thickness of 0.127

http://doi.org/10.18080/jtde.v8n3.299

mm. Each antenna element has a length of 3.12 mm, and a width of 2.6 mm. The feeding gap was cut at 0.793 mm deep along the length of the antenna. The width of the microstrip feeding line is 0.391 mm, leaving a gap of length 0.196 mm at each side of the line. Furthermore, the feeding line is 2.405 mm long. In the 2×2 array, the separation between the two elements horizontally measured from centre to centre is 6.5 mm, which translates to 3.38 mm from edge to edge. The vertical separation used is 6 mm from centre to centre: that is, 3.4 mm from edge to edge. Three quarter-wave transformers were used to connect the array; each has a length of 2.924 mm and a width of 0.222 mm. Also, a total of nine triangles were cut to reduce power losses. All triangles are equilateral, with side length of 0.26174 mm at the quarter-wave transformers, and 0.26174 mm at the other 50Ω lines.

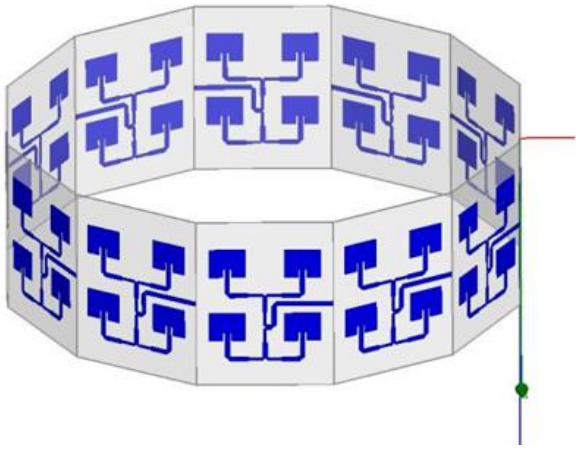

Figure 4. The Final Antenna Design.

The total size of each array is 15.392 mm long by 11.9 mm wide and 0.127 mm thick. Figure 4 depicts the design of the final antenna prototype. With each side of 11.9 mm, the circumcircle diameter of the polygon is 45.978 mm, and the inner circle diameter is 44.411 mm. The total area of the polygon is 1330.203 mm² (counting the gap in the middle as part of the antenna). Moreover, the antenna maintains its low profile by the use of the microstrip feeding technique.

Simulation Results of the MIMO Antenna Array

The achieved return loss by our proposed design is depicted in Figure 5. It is evident in Figure 5 that the lowest point in the graph occurs at a frequency of 38.1141 GHz. The return loss at that frequency is -17.7122 dB; this value translates to an antenna that radiates most of its input power at that frequency. In addition, in this graph the -3 dB point occurs first at a frequency of 37.2730 GHz and crosses it again at 38.7390 GHz. Thus, the bandwidth of this antenna is 1.4660 GHz. In addition to that, the 10 dB bandwidth of the antenna is 0.509 GHz. Figure 6 shows the 3D gain polar plot, where the figure shows the gain of the antenna in the direction of the excited port is 14.358 dB. In addition, there exist side lobes with a low

http://doi.org/10.18080/jtde.v8n3.299

gain of about 5 dB. This pattern can be rotated as desired in increments of 30°along θ-axis. The gain values are the same for all sides. Since there are twelve sides, each with a coverage range of about 60°, this enables the antenna to scan 360°with minimal overlapping and dead zones. Figure 7 shows the return loss of all mutual terms when a single side is excited. This figure demonstrates the crucial isolation between elements, where the self-term starts at 0 dB and quickly drops below -10 dB around the operating frequency, then rises back to 0 dB. All other mutual terms have very low return loss values that do not affect the radiation of the antenna. In HFSS, realized gain value differs from traditional gain described in this paper; this is due to the fact that the realized gain accounts for all losses that might affect the obtained result. Hence, when plotting the sector covered by each side, it is fair to account for all losses. Figure 8 is a plot of the azimuth plane realized gain when the antenna face facing 0° is excited. Figure 8 shows a beam width of 58°.

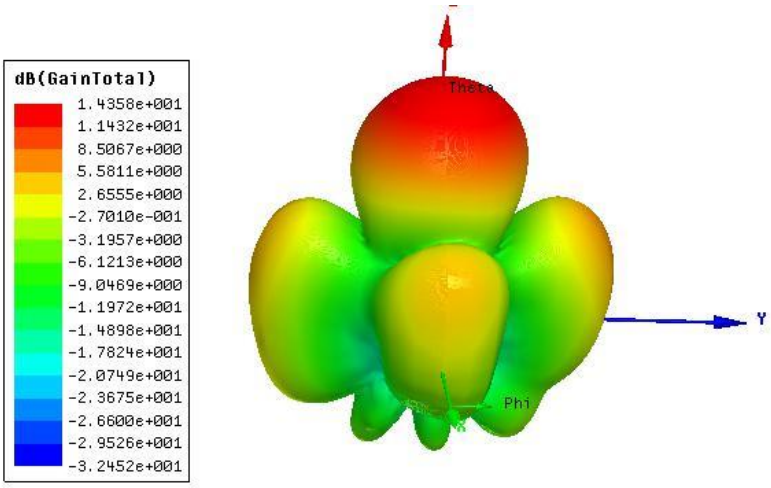

Figure 5. 3D Gain Polar Plot.

With each antenna array angled at 30°, this ensures that all areas around the antenna are covered. The figure also shows two side lobes, each with a gain of less than 2 dB, which is unlikely to interfere with any transmission or reception of signals. To show the maximum number of sectors and the coverage range, all arrays were excited individually and overlaid into the same plot, as depicted in Figure 9, which shows all the sectors. The coverage of the 360 degrees is achieved as the 12 faces are excited individually. As seen above, each sector can cover a beam of 58° to end up with 12 beams covering the 360 degrees. Despite the fact that some areas overlap between two adjacent sectors, the methodology of the arrayed antenna achieved the goal of transmitting and receiving signals in all directions.

http://doi.org/10.18080/jtde.v8n3.299

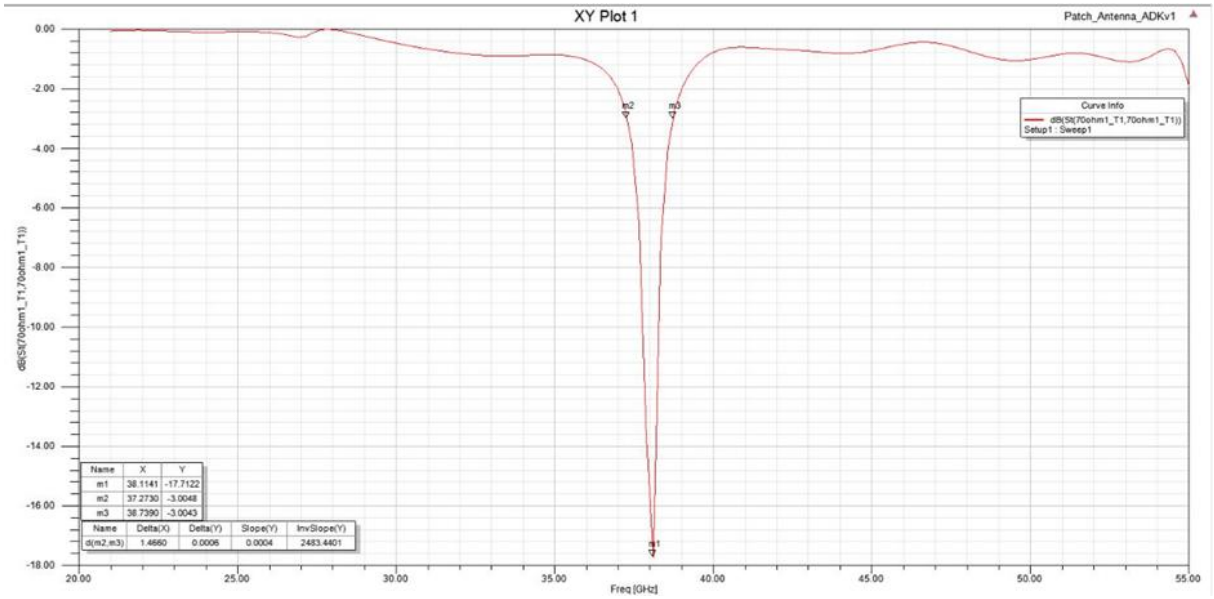

Figure 6. The Return Loss.

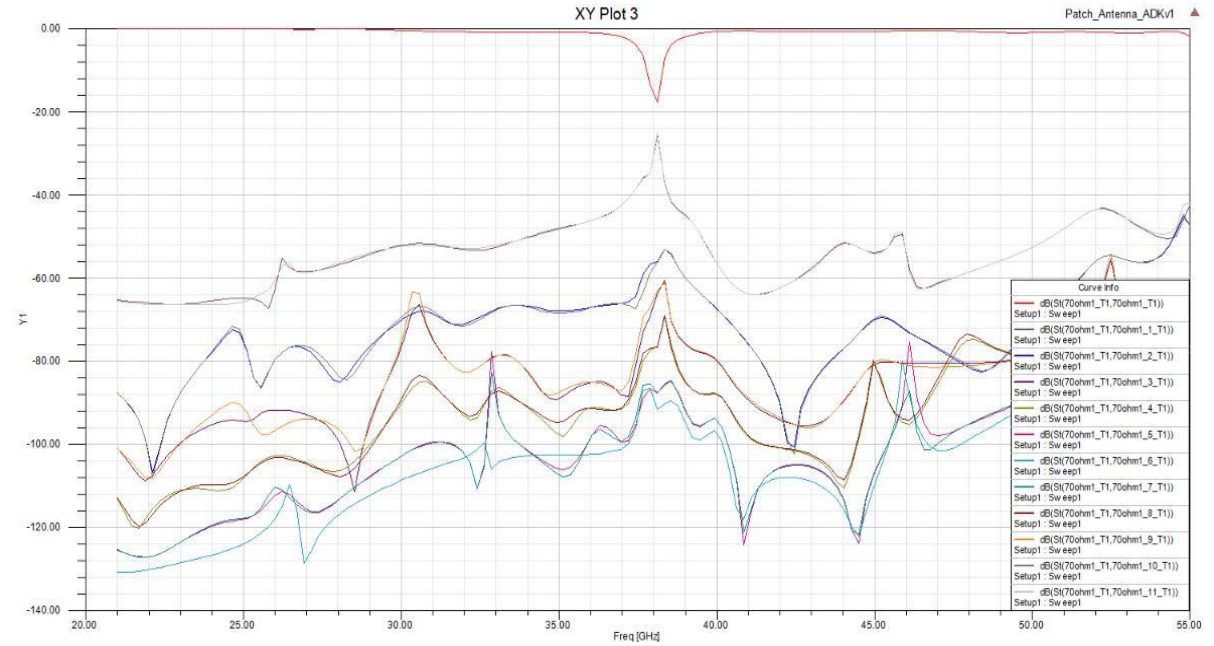

Figure 7. Return Loss Showing Self-Terms and Mutual-Terms.

http://doi.org/10.18080/jtde.v8n3.299

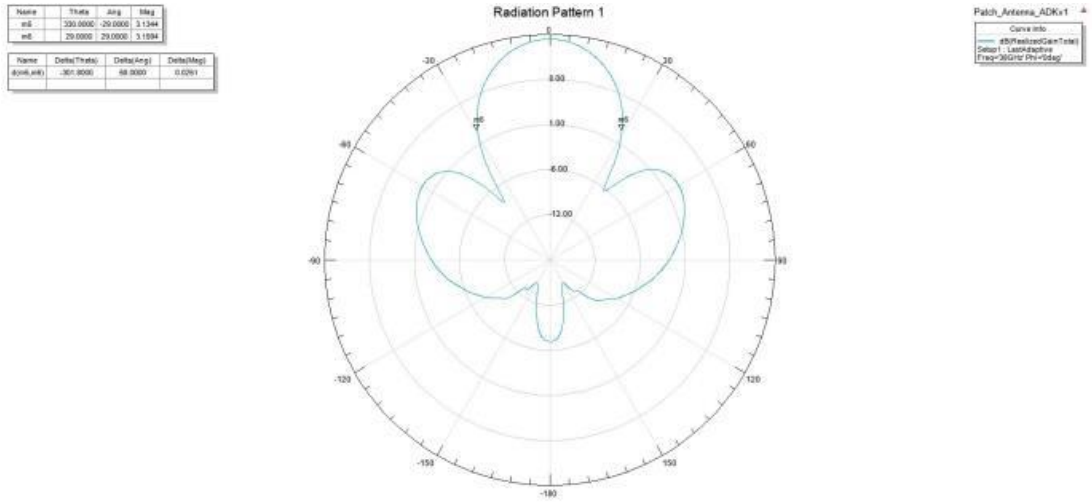

Figure 8. Realized Gain in Azimuth Plane.

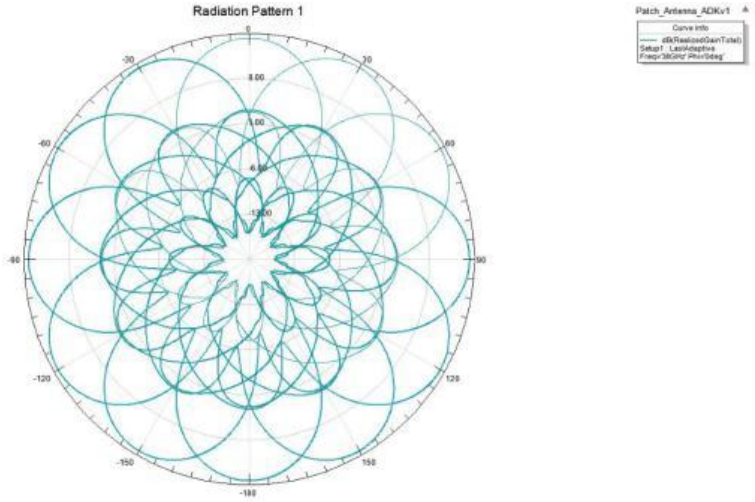

Figure 9. Azimuth Plane Showing All Sectors.

Conclusion

In this paper, the structure of a compact and low-profile efficient high gain sectoring antenna array operating at a mmWave frequency of 38 GHz was presented. The design of this compact antenna uses a 2×2 microstrip antenna array of size 11.9×15.3 mm². At this operating frequency of 38 GHz, we achieved a high gain of 14.58 dB, a return loss of -17.7 dB, and a wide impedance bandwidth of 500 MHz. This 2×2 microstrip antenna array is duplicated twelve times around an angle of 30°forming a dodecagon. Each sector can cover a beam of 58° to end up with 12 beams covering the 360 degrees. When compared to antenna designs with a similar purpose in the literature, our design operated at the desired 5G frequency of 38 GHz and had a noticeable reduction in size, in addition to an increase in gain of about 1.5 dB. Our designed antenna is suited to beamforming or switched-beam MIMO technology applications that require compact and low-profile antennas, such as MN systems in 5G vehicular communications.

http://doi.org/10.18080/jtde.v8n3.299

References

Al Issa, H., Khraisat, Y., & Alghazo, F. (2020). Bandwidth Enhancement of Microstrip Patch Antenna by Using Metamaterial. *International Journal of Interactive Mobile Technologies (iJIM)*, *14*(1), 169.175. http://doi.org/10.3991/ijim.v14i01.10618

Ali, M., Haraz, O., & Alshebeili, S. (2016). Design of a Dual-Band Printed Slot Antenna with Utilizing a Band Rejection Element for the 5G Wireless Applications. In *2016 IEEE International Symposium on Antennas and Propagation (APSURSI)*, IEEE, 1865–1866.

Ali, M., & Sebak, A. (2016). Design of Compact Millimeter Wave Massive MIMO Dual-Band (28/38 GHz) Antenna Array for Future 5G Communication Systems. In *2016 17th International Symposium on Antenna Technology and Applied Electromagnetics (ANTEM)*, IEEE, 1–2.

Al-Tarifi, M., Sharawi, M., & Shamim, A. (2018). Massive MIMO Antenna System for 5G Base Stations with Directive Ports and Switched Beamsteering Capabilities. *IET Microwaves, Antennas Propagation*, *12*(10): 1709–1718. http://doi.org/10.1049/iet-map.2018.0005

Chen, Z., & Zhang, Y. (2013). FR4 PCB Grid Array Antenna for Millimeter-Wave 5G Mobile Communications. In *2013 IEEE MTT-S International Microwave Workshop Series on RF and Wireless Technologies for Biomedical and Healthcare Applications (IMWS-BIO)*, IEEE, 1–3.

Fadamiro, A. O., Famoriji, O. J., Zakariyya, R. S., Lin, F., Somefun, O. A., Ogunti, E. O., Apena, W. O., & Dahunsi, F. M. (2019). Temperature Variation Effect on a Rectangular Microstrip Patch Antenna. *International Journal of Online and Biomedical Engineering (iJOE)*, *15*(5), 101-118.

Hong, W., Jiang, Z. H., Yu, C., Chen, P., Yu, Z., Zhang, H., Yang, B., Pang, X., Cheng, Y., Zhang, Y., Chen, J., & He, S. (2017). Multibeam Antenna Technologies for 5G Wireless Communications. *IEEE Transactions on Antennas and Propagation*, *65*(12), 6231–49. http://doi.org/10.1109/TAP.2017.2712819

Kim, J., Chung, H., Noh, G., Choi, S.-W., Kim, I., & Han, Y. (2019). Overview of Moving Network System for 5G Vehicular Communications. In *2019 13th European Conference on Antennas and Propagation (EuCAP)*, Krakow, Poland, 1–5.

Mattisson, S. (2018). An Overview of 5G Requirements and Future Wireless Networks: Accommodating Scaling Technology. *IEEE Solid-State Circuits Magazine*, *10*(3), 54–60. http://doi.org/10.1109/MSSC.2018.2844606

Milligan, T. A. (2005). *Modern Antenna Design*. 2nd ed. John Wiley & Sons, Inc.

Mishra, R., Kuchhal, P., & Kumar, A. (2015). Effect of Height of the Substrate and Width of the Patch on the Performance Characteristics of Microstrip Antenna. *International Journal of Electrical and Computer Engineering*, *5*(6), 1441-1445. http://doi.org/10.11591/ijece.v5i6.pp1441-1445

Muirhead, D., Imran, M., & Arshad, K. (2016). A Survey of the Challenges, Opportunities and Use of Multiple Antennas in Current and Future 5G Small Cell Base Stations. *IEEE Access*, *4*, 2952–2964. http://doi.org/10.1109/ACCESS.2016.2569483

Rappaport, T. S., Xing, Y., MacCartney, G. R., Molisch, A. F., Mellios, E., & Zhang, J. (2017). Overview of Millimeter Wave Communications for Fifth-Generation (5G) Wireless Networks—With a Focus on Propagation Models. *IEEE Transactions on Antennas and Propagation* 65(12), 6213–6230. http://doi.org/10.1109/TAP.2017.2734243

Rogers Corporation. (2018). *RT/duroid® 5870 /5880 High Frequency Laminates*. https://www.rogerscorp.com/-/media/project/rogerscorp/documents/advanced-connectivity-solutions/english/data-sheets/rt-duroid-5870---5880-data-sheet.pdf.

Sahoo, B. P. S., Chou, C., Weng, C., & Wei, H. (2019). Enabling Millimeter-Wave 5G Networks for Massive IoT Applications: A Closer Look at the Issues Impacting Millimeter-Waves in Consumer Devices Under the 5G Framework. *IEEE Consumer Electronics Magazine*, *8*(1), 49–54. http://doi.org/10.1109/MCE.2018.2868111

Samarthay, V., Pundir, S., & Lal, B. (2014). Designing and Optimization of Inset Fed Rectangular Microstrip Patch Antenna (RMPA) For Varying Inset Gap and Inset Length. *International Journal of Electronic and Electrical Engineering*, *7*(9), 1007–1013.

Verma, S., Mahajan, L., Kumar, R., Saini, H. S., & Kumar, N. (2016). A Small Microstrip Patch Antenna for Future 5G Applications. In *2016 5th International Conference on Reliability, Infocom Technologies and Optimization (Trends and Future Directions) (ICRITO)*, IEEE, 460–463. http://doi.org/10.1109/ICRITO.2016.7784999

Wu, Z., Wu, B., Su, Z. & Zhang, X. (2018). Development Challenges for 5G Base Station Antennas. In *2018 International Workshop on Antenna Technology (IWAT)*, 1–3. http://doi.org/ 10.1109/IWAT.2018.8379163

Yaacoub, E., Husseini, M., & Ghaziri, H. (2016). An Overview of Research Topics and Challenges for 5G Massive MIMO Antennas. In *2016 IEEE Middle East Conference on Antennas and Propagation (MECAP)*, Beirut, 1–4. http://doi.org/10.1109/MECAP.2016.7790121